ACS OMEGA

Open Access



http://pubs.acs.org/journal/acsodf

Article

# Ultrasensitive Fluorescence Detection of Ascorbic Acid Using Silver Ion-Modulated High-Quality CdSe/CdS/ZnS Quantum Dots

Xingchang Lu, Zheng Wang, Jianxiu Wang, Yang Li,* and Xiaoqi Hou*

Cite This: *ACS Omega* 2024, 9, 27127−27136

Read Online

ACCESS | Metrics & More | Article Recommendations | Supporting Information

**ABSTRACT:** Improving the sensitivity of the fluorescence method for the detection of bioactive molecules is crucial in biochemical analysis. In this work, an ultrasensitive sensing strategy was constructed for the detection of ascorbic acid (AA) using high-quality 3-mercaptopropionic acid-capped CdSe/CdS/ZnS quantum dots (MPA-CdSe/CdS/ZnS QDs) as the fluorescent probe. The prepared water-soluble QDs exhibited a high photoluminescence quantum yield (PL QY) of up to 96%. Further, the fluorescence intensity of the QDs was intensively quenched through the dynamic quenching of $Ag^+$ ions due to an efficient photoinduced electron transfer progress. While the existence of AA before adding $Ag^+$ ions, $Ag^+$ ions were reduced. Thus, the interaction of the QDs and $Ag^+$ ions was destroyed, which led to the fluorescence distinct recovery. The detection limit of AA could be as low as 0.2 nM using this sensing system. Additionally, most relevant small molecules and physiological ions had no influence on the analysis of AA. Satisfactory results were obtained in orange beverages, showing its great potential as a meaningful platform for highly sensitive and selective AA sensing for clinical analysis.

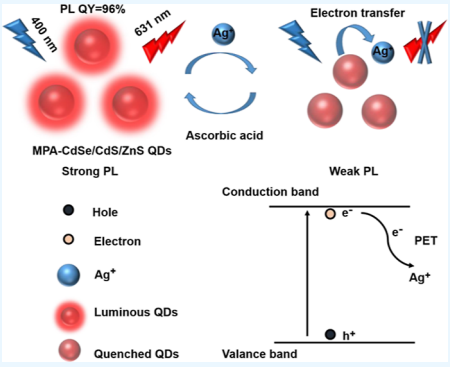


## 1. INTRODUCTION

Ascorbic acid (AA) plays an irreplaceable role in some physiological processes, including functioning as a free radical scavenger, collagen synthesis, and human disease prevention.[1−3] As a crucial and resultful antioxidant, AA can hold back reactive oxide species free radical-caused diseases such as Alzheimer's disease.[4] According to reports in the literature, the concentration of AA in the human body is dramatically related to multiple diseases. The lack of AA can give rise to scurvy. However, the amount of AA is too high, which contributes to stomach convulsion.[5,6] Given the significance of AA, there is an urgent need to establish a rapid and sensitive sensing strategy for the quantitative determination of AA.

At present, a variety of methods have been put forward for AA testing, including electrochemical,[7−10] chemiluminescence,[11] electrochemiluminescence,[12] high-performance liquid chromatography,[13] colorimetric,[14−16] and so on. However, most of these methods are limited by the complexity of operations, time consumption, and expensive equipment. Compared with these methods, fluorescent sensors have attracted considerable attention owing to their intrinsic advantages of simplicity, real-time imaging, rapid analysis, and excellent sensitivity.[17−19] At present, researchers have paid lots of efforts to pullulate fluorescent probes for measurement of AA, including organic fluorescence dyes,[20,21] metallic clusters (e.g., Au/Cu nanoclusters),[22−24] graphene quantum dots (QDs),[25−28] and carbon QDs.[29−33] In comparison with organic chromophores and nanoclusters, QDs have been generally researched as fluorescent probes owing to their tunable emission spectra as well as antiphotodegradation. Nonetheless, most of these QD fluorescence probes are fabricated via aqueous-phase synthesis routes, resulting in relatively low emission efficiency and a wide fluorescence spectrum due to interior electron−hole traps.[34] It is widely known that the excellent optical properties of QD-based fluorescent probes are a guarantee for highly sensitive sensing. Consequently, the development of a convenient and ultrasensitive method for detection of AA based on QDs with ideal optical properties is urgently demanded for further investigation.

Semiconductor quantum dots (SQDs) as important luminescent materials have gained considerable attention for their practical applications such as lasers,[35] light-emitting diodes,[36,37] and biosensors[38] owing to their size-dependent luminescence, high PL QY, and long fluorescence lifetime.[39] Generally, the high-quality SQDs are synthesized in nonpolar organic solvents with hydrophobic ligands on their surfaces, limiting their direct application in biological assays.[40] To make the SQDs soluble in water, some strategies have been proposed for constructing water-soluble SQDs, including encapsulation in amphipathic micelles,[41] coating with $SiO_2$,[42,43] and surface ligand exchange.[44−46] Unfortunately, almost all reported

Received: February 1, 2024
Revised: May 14, 2024
Accepted: May 24, 2024
Published: June 13, 2024

**Scheme 1. Schematic Illustration of (a) Synthesis of the CdSe/CdS/ZnS Core/Shell/Shell QDs and (b) Its Application for Fluorescence Turn-On Detection of AA**

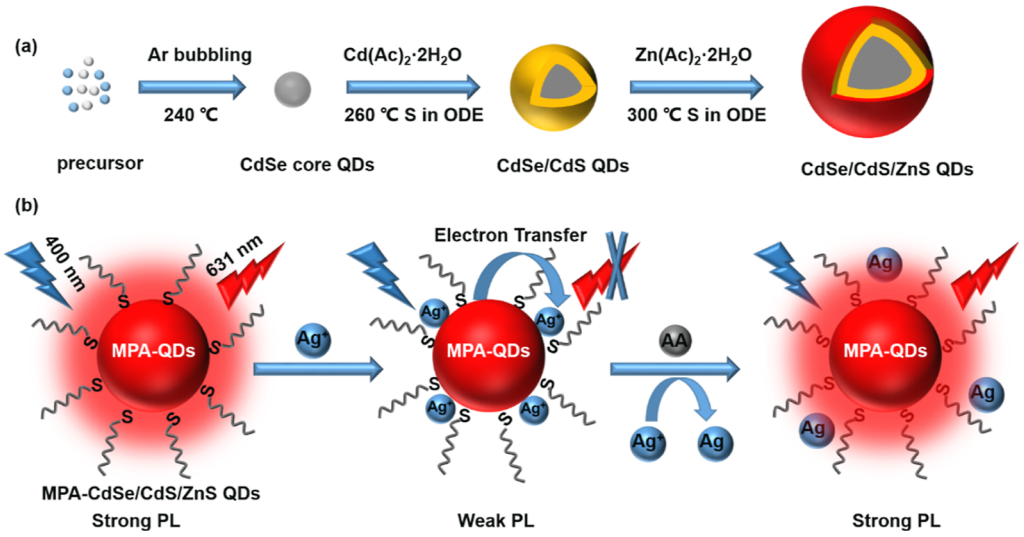


methods inevitably give rise to the significant PL QY decrease compared to the pristine hydrophobic SQDs due to the formation of surface damage or ligand loss. Thus, the design and synthesis of water-soluble SQDs with near-unity PL QY are still a challenging task.

In this work, we managed to overcome the problem of the PL QY loss during phase transfer by an optical inorganic structure. The designed trap-free CdSe/CdS/ZnS QDs with nearly perfect optical properties were prepared in a nonpolar solvent and then ligand-exchanged with 3-mercaptopropionic acid (MPA), converting the hydrophobic QDs to be hydrophilic. Notably, the as-synthesized water-soluble QDs exhibited a high PL QY of 96% and monoexponential PL decay curves in aqueous media, originating from the isolation of the exciton from the defect at the surface by outermost CdS and ZnS shells. Furthermore, we constructed an ultrasensitive and convenient "on−off−on" fluorescent sensor for AA detection utilizing the $Ag^+$-mediated fluorescence signal of the QDs. The fluorescence of the QDs was efficiently quenched by $Ag^+$ ions, which followed an electron-transfer quenching mechanism from the QDs to $Ag^+$. However, the pre-existing AA could generally maintain the PL intensity of the QDs through the special redox reaction between AA and $Ag^+$ ions. Thus, an ultrasensitive QD-based fluorescent probe for detection AA was developed. The detection limit was as low as 0.2 nM. This work demonstrated that the water-soluble QDs had great potential to serve as a high-efficiency fluorescent probe.

## 2. EXPERIMENTAL SECTION

**2.1. Materials.** Silver nitrate ($AgNO_3$), bovine serum albumin (BSA), cadmium oxide (CdO), sulfur powder (S), selenium powder (Se), 1-octadecene (ODE), 3-mercaptopropionic acid (MPA), and tetramethylammonium hydroxide (TMAH) were purchased from Sigma-Aldrich Chemical Co. (USA). AA was purchased from Shanghai Sangon Biotechnology Co.Ltd. (Shanghai, China). Urea, dopamine (DA), adenosine triphosphate (ATP), glycine (Gly), citric acid, potassium chloride (KCl), glucose (Glu), uric acid, ferric chloride hexahydrate ($FeCl_3·6H_2O$), sodium chloride (NaCl), calcium chloride ($CaCl_2$), sodium hydroxide (NaOH), and magnesium chloride were bought from Sinopharm Chemical Reagent Co., Ltd. (China).

**2.2. Characterizations.** Transmission electron microscopy (TEM) images were obtained using a Hitachi 7700 microscope (Tokyo, Japan). The EDS spectrum was received through a Thermo Fischer Talos F200x high-resolution TEM (Czech Republic). FTIR spectra were obtained on a Thermo Nicolet iS50 spectrometer (Madison, USA). XPS measurements were performed using the ESCALAB 250Xi (Thermo Fisher Scientific, USA). The fluorescence spectra and lifetime were carried out using an FS5 spectrometer (Livingston, UK), and the excitation wavelengths were 400 and 450 nm, respectively. The absolute PL QY of the hydrophilic QDs was tested by a QE65000 spectrometer and assembled with an integrating sphere of an Ocean Optics FOIS-1 integrating sphere. The ultraviolet−visible absorption spectra were recorded via an Agilent Cary 60. The hydrodynamic diameter and zeta potential were tested at neutral pH conditions by a Malvern Zen 3600 Zetasizer (Malvern, Instruments Ltd., UK). Milli-Q water (18.25 MΩ cm) was used throughout the study.

**2.3. Synthesis of CdSe QDs.** First, 0.1 mmol of CdO, 0.28 mmol of myristic acid, and 4 mL of ODE were added to a 25 mL flask. The temperature was heated to 250 °C and held for 30 min. 1 mL of Se powder in the ODE (0.6 mmol) was rapidly injected. The reaction temperature was cooled to 240 °C. After 5 min, the Se powder in the ODE (0.1 mmol) was drop by drop instilled into the solution until CdSe QDs with the needed size were obtained.

**2.4. Synthesis of CdSe/CdS QDs.** First, 2 mmol of oleic acid, 0.7 mmol of $Cd(Ac)_2·2H_2O$, 0.7 mmol of capric acid, and 4 mL of ODE were loaded into a 25 mL flask. Argon pumping was carried out for 15 min, and the temperature was heated to 160 °C. 500 μL of CdSe core QDs was apace injected into the solution. Afterward, the temperature was heated to 260 °C. The sulfur dissolved in ODE (0.1 M) was instilled into the flask until CdSe/CdS QDs with a needed CdS shell thickness were obtained.

**2.5. Synthesis of CdSe/CdS/ZnS QDs.** First, 0.4 mmol of capric acid, 0.4 mmol of $Zn(Ac)_2·2H_2O$, 1 mmol of oleic acid, and 4 mL of ODE were added into a 25 mL flask. Argon pumping was carried out for 20 min, and the temperature was


https://doi.org/10.1021/acsomega.4c01045
ACS Omega 2024, 9, 27127−27136

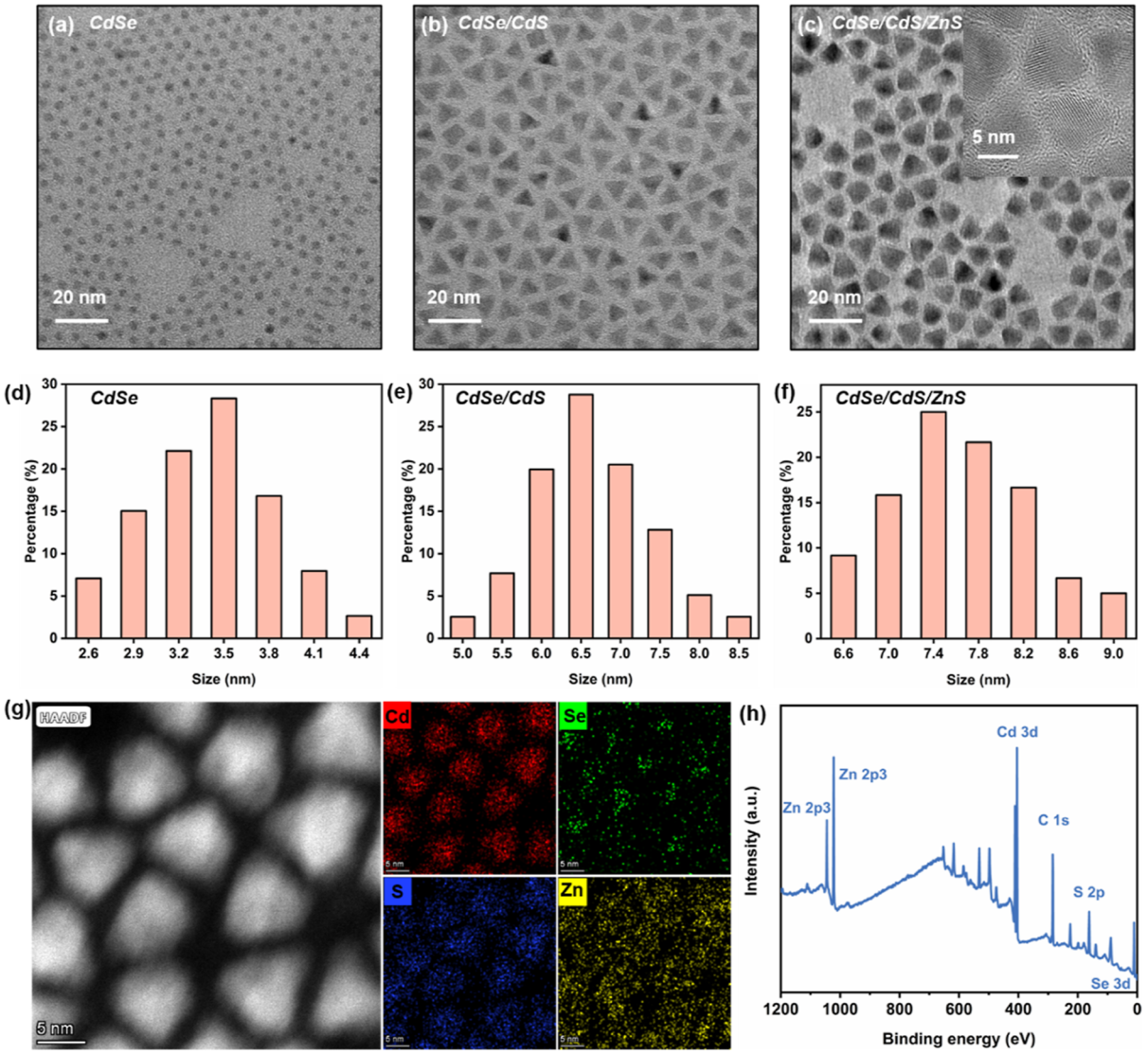


**Figure 1.** TEM images and the statistical particle size distribution diagrams of (a,d) CdSe QDs, (b,e) CdSe/CdS QDs, and (c,f) CdSe/CdS/ZnS QDs. The high-resolution TEM image (the inset of (c)) of CdSe/CdS/ZnS QDs. (g) Elemental distribution mapping of hydrophobic CdSe/CdS/ZnS QDs. (h) FTIR of hydrophobic CdSe/CdS/ZnS QDs before and after surface ligand exchange.

heated to 150 °C. 500 $\mu$L of CdSe/CdS QDs was apace loaded into the solution. Afterward, the temperature was heated to 300 °C. The sulfur dissolved in ODE (0.2 M) was dropwise added into the reaction flask. The reaction was proceeded until CdSe/CdS/ZnS QDs with an appropriate ZnS shell thickness were obtained.

**2.6. Synthesis of the MPA-CdSe/CdS/ZnS QDs by Surface Ligand Exchange.** 1 mL of purified CdSe/CdS/ZnS QDs was dissolved in chloroform, and then 60 $\mu$L of MPA was appended to the above solution. After being ultrasounded for 10 min and then centrifuged, the precipitate was washed more than twice using hexane. Afterward, the organic solvent was fully removed in an argon atmosphere. In the end, the powder was dissolved in water, and the pH was adjusted to 12 using TMAH.

**2.7. Fluorescence Determination of AA.** For the determination of AA, typically, 10 $\mu$L of the MPA-CdSe/CdS/ZnS QDs was added to AA solutions with different concentrations, Then, 3 $\mu$L of $Ag^+$ (400 $\mu$M) was appended to the solution. The final concentrations of AA were 0, 1, 10, 20, 30, 45, 50, 70, 100, 150, and 250 nM. The final solution volume was set as 3 mL by using deionized water. Notably, the pH value was fixed at 11. After reaction for 15 min, the fluorescence spectra of the solutions were recorded for the quantitative analysis of AA. The limit of detection was calculated through the formula LOD = $(3\sigma)/k$ (1), where $\sigma$ is the blank sample standard deviation ($n$ = 6) and $k$ is the fitted curve slope of change in the PL intensity against the AA concentration. The PL measuring parameter and slot widths were both set as 5 nm, and the excitation wavelength was 400 nm.

**2.8. Analysis of Real Samples.** The orange beverages were purchased from a supermarket as real samples. First, the beverage was centrifuged and then filtered via a 0.45 $\mu$M microporous membrane. Subsequently, the resulting solution was diluted at different times with deionized water (pH = 11) to confirm the feasibility for detecting AA in real samples. The procedure was the same as that mentioned in Section 2.7.



https://doi.org/10.1021/acsomega.4c01045
ACS Omega 2024, 9, 27127−27136

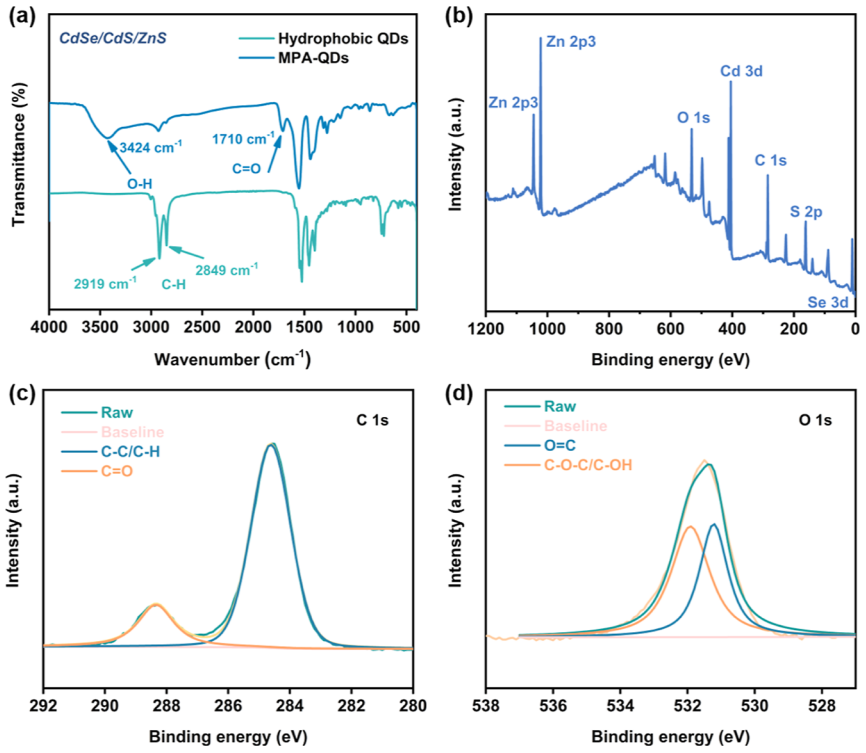


**Figure 2.** (a) FTIR spectra of hydrophobic QDs before and after surface ligand exchange. (b) XPS full survey spectra of hydrophilic QDs. High-resolution spectra of (c) C 1s and (d) O 1s.

## 3. RESULTS AND DISCUSSION

**3.1. Structural Characterization of QDs.** The preparation of QDs and PL response principle are illustrated in Scheme 1. The high-quality CdSe/CdS/ZnS QDs had been prepared by the high-temperature hot injection method.[47] Notably, CdS shells were selected as the transition layer, originating from the crystal strain at the core−shell interface slightly. Additionally, the core/shell structure QDs could passivate the surface defects of the CdSe core, which could significantly improve the PL QY.

TEM images and statistical size distribution histograms are shown in Figure 1a−f. The as-prepared QDs were nearly monodisperse in size (Figure S1). After the addition growth of wide-bandgap CdS and ZnS shells, the size of the QDs gradually increased. The average particle sizes were 3.5, 6.4, and 7.5 nm. Moreover, the high-resolution TEM image (inset of Figure 1c) showed that the as-prepared CdSe/CdS/ZnS QDs had an ideal crystalline structure. As shown in Figure S2, five diffraction peaks were observed, respectively, indexing to the (111), (200), (220), (222), and (311) planes, suggesting that the as-prepared QDs had good crystallinity. Moreover, the elemental composition of the QDs was identified by EDS, which indicated that the four characteristic elements, Cd, S, Zn, and Se, are shown in Figure 1g. The Se element almost existed in the core inside, while the outer shell had Zn and S elements, demonstrating that the shell epitaxial growth process was controlled. In addition, the elemental composition of the QDs was also identified using XPS. The results from Figure 1h exhibited four representative peaks like Cd, Se, S, and Zn, suggesting the successfully synthesized CdSe/CdS/ZnS QDs.

**3.2. Surface Ligand Exchange.** The mercapto groups could interact with the metal Zn atom via the formation of a metallic mercaptan bond (Zn-SR), and further, the carboxyl groups provided excellent water solubility. The surface ligand-exchange process was demonstrated by Fourier transform infrared (FTIR) spectra and XPS. Notably, the characteristic absorption bands at 2919 and 2849 $cm^{-1}$ were originated from the C−H vibration of the long-chain hydrophobic alkyl ligand, while the C−H intensity was significantly reduced after ligand exchange. The S−H stretching vibration peaks were not found due to the formation of Zn-SR (Figure 2a). These results indicated that MPA successfully bound to the surface of the QDs via sulfhydryl groups. To further confirm the surface chemical states of the QDs, XPS analysis was executed. The XPS survey spectra exhibited peaks like Zn 2p, C 1s, Se 3d, Cd 3d, S 2p, and O 1s (Figure 2b). Furthermore, the XPS spectra of C 1s illustrated two species of C−C/C−H and C═O, corresponding to 284.6 and 288.3 eV, respectively (Figure 2c). According to Figure 2d, the analysis of O 1s showed C═O, C−O−C, and C−OH, which corresponded to 531.2 and 531.9 eV, respectively. The results further demonstrated that MPA had been successfully modified on the surface of the QDs.

**3.3. Optical Properties of QDs.** The optical properties of the obtained QDs were measured. First, as shown in Figure 3a, the CdSe core QDs exhibited a distinct first exciton absorption peak and a narrow PL emission spectrum. Additionally, a strong red-shift of first exciton absorption and fluorescence emission peak was discovered, which was consistent with the growth of the CdS shells onto the CdSe core QDs (Figure S3a). When ZnS shells were further epitaxially grown, the absorption and PL spectra continuously were further red-shifted (Figure S4a). Notably, the emission peak was narrow and symmetric, further confirming a narrow size distribution. In order to further recognize the carrier dynamics, we recorded the transient PL spectra during the process of shell growth. The average PL lifetime gradually increased with the increase of CdS and ZnS shell thickness (Figures S3b and S4b), suggesting the perfect passivation of surface trap. Most


https://doi.org/10.1021/acsomega.4c01045
ACS Omega 2024, 9, 27127−27136

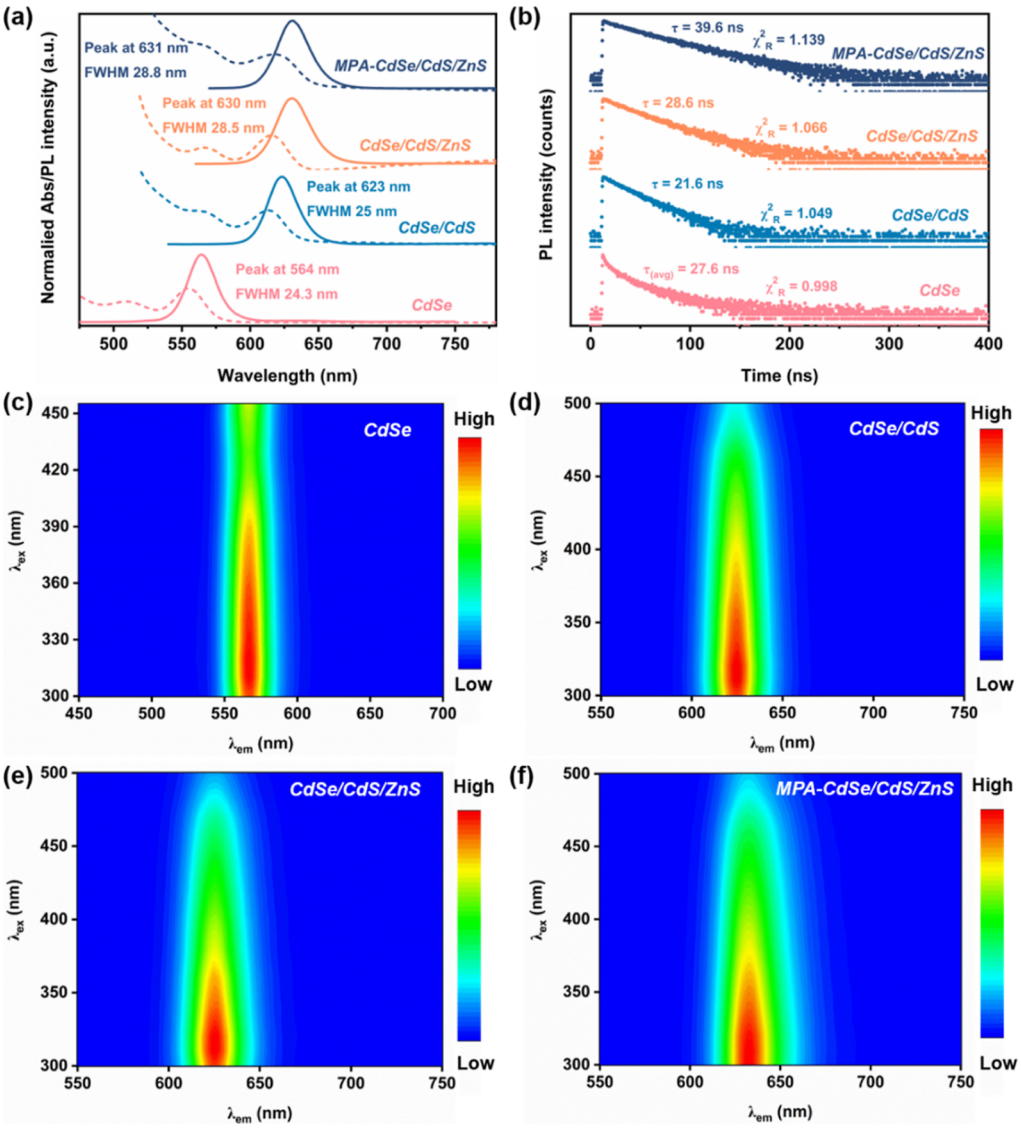


**Figure 3.** (a) Normalized UV−vis absorption and fluorescence spectra of QDs. (b) PL decay curves of QDs. $\tau$ and $\chi_R^2$ represented the monoexponential fitting lifetime and goodness of fit, respectively. (c−f) Three-dimensional fluorescence mapping of QDs.

importantly, the transient PL spectra of the water-soluble QDs showed a monoexponential function (Figure 3b). The results indicated that the fluorescence emission was due to band-edge excitons, benefiting from the CdS and ZnS shells passivating the core to reduce surface defects and sensitivity to the environment. The absolute fluorescence QY of hydrophilic QDs was calculated to be as high as 96% (Figure S5). To further explain the excellent optical properties of QDs, three-dimensional fluorescence mapping was executed (Figure 3c−f). The fluorescence spectra showed that a high concentrated center, indicating narrow band-edge PL emission and originating from the CdS and ZnS shells acting as the surface passivation layers, enhanced the PL stability of the core QDs. Additionally, the stability of the hydrophilic QDs was investigated (Figure S6a). The results showed that the PL intensity did not significantly fluctuate upon ultraviolet irradiation, illustrating their excellent photostability. To evaluate thermal stability, the QD aqueous solution was heated to different temperatures (0−50 °C), and changes in the PL intensity were recorded (Figure S6b). The PL intensity did not change significantly, indicating the remarkable thermal stability of the QDs. These results clearly suggested that the QDs with perfect PL performances could be constructed as a fluorescent probe used in a biological system.

**3.4. Feasibility and Optimization of the Detection Condition.** The feasibility of QDs as nanosensors to detect AA was investigated (Figures 4a and S7). After the addition of $Ag^+$ ions to the QD solution, the PL intensity of the QDs was distinctively quenched. It was interesting that previous addition of AA to QDs in the presence of $Ag^+$ could partially restore the fluorescence, demonstrating that the QDs/$Ag^+$ system could serve as an "on−off−on" fluorescence sensor for AA determination. To achieve optimal performances, the experimental conditions were explored. The effects of $Ag^+$ ion concentrations on the fluorescence intensity of the QD solution were investigated (Figure 4b). The PL intensity of the QDs gradually decreased with the increase of $Ag^+$ concentration and reached a plateau stage at 0.3 $\mu$M. The fluorescence-quenched efficiency was as high as 95% (the inset of Figure 4b), indicating that $Ag^+$ have excellent fluorescence quenching ability. Fluorescence-quenched efficiency was calculated using quenching efficiency = $(F_0 - F)/F_0$ (2),


https://doi.org/10.1021/acsomega.4c01045
ACS Omega 2024, 9, 27127−27136

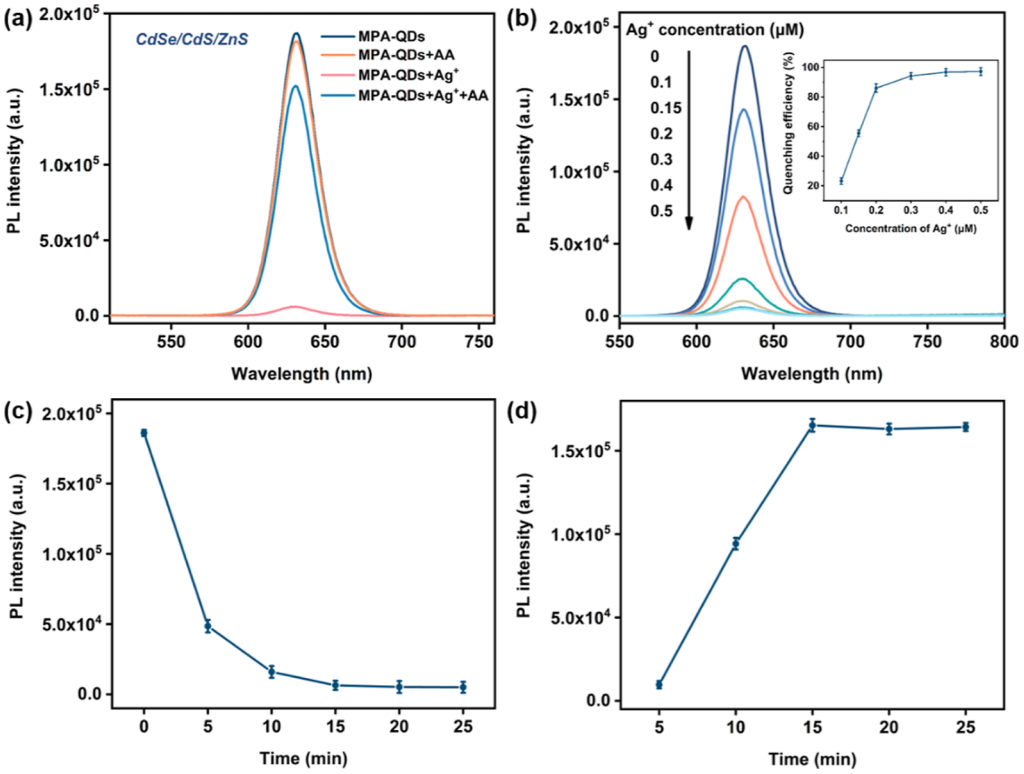


**Figure 4.** (a) Feasibility of the sensor platform for AA detection. (b) Fluorescence spectra ($\lambda_{ex}$ = 400 nm) of the QDs in the presence of $Ag^+$ ions with various concentrations (0, 0.1, 0.15, 0.2, 0.3, 0.4, and 0.5 $\mu$M). The inset shows the corresponding fluorescence quenching rate. Influence of the incubation time on (c) fluorescence quenching with the addition of 0.3 $\mu$M of $Ag^+$ ions and (d) recovery upon the addition of 200 nM of AA.

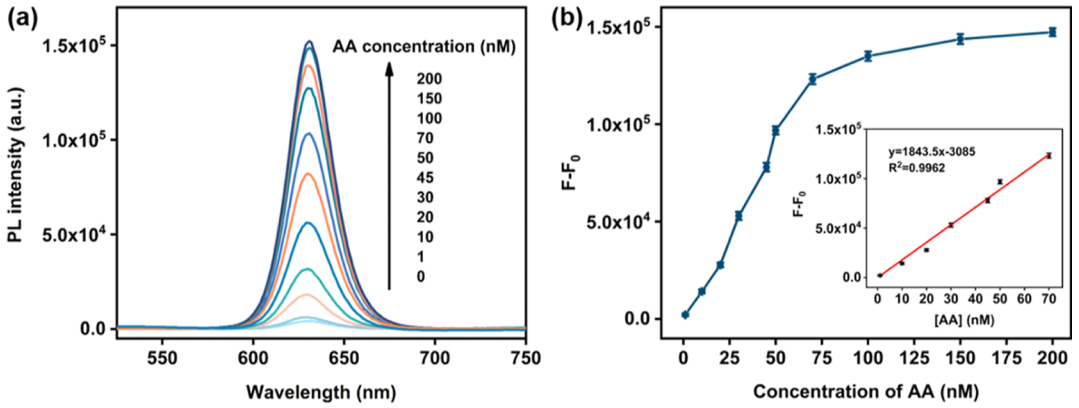


**Figure 5.** (a) Fluorescence spectra ($\lambda_{ex}$ = 400 nm) of the QDs/$Ag^+$ system upon exposure to different concentrations of AA. The concentrations of AA from bottom to top were 0, 1, 10, 20, 30, 45, 50, 70, 100, 150, and 200 nM. (b) Dependence of the PL intensity on the concentration of AA. The inset showed the linear relationship with the concentrations of AA from 1 to 70 nM.

where $F$ and $F_0$ are the PL intensity of the QDs in the presence and absence of $Ag^+$ ions, respectively. Moreover, the effect of pH on the performance of the sensors was investigated. As shown in Figure S8, the optimal detection performance could be obtained under a pH value of 11. Further, the effects of reaction time with $Ag^+$ ions (Figure 4c) and AA (Figure 4d) on the PL intensity of the QDs were explored. The time of fluorescence quenching and recovery both was chosen as 15 min.

### 3.5. Analytical Performance of the Sensing System.

The detection performance of the QDs/$Ag^+$ system for AA was further investigated under optimal experiment conditions. Figure 5a shows that the intensity of the QDs was gradually increased with enhancing the AA concentration, which may result from the fact that $Ag^+$ ions were reduced by AA. The inset of Figure 5b represents the linear fitted curve between intensity and the AA concentration ranging from 1 to 70 nM. In the figure, $F$ and $F_0$ denoted the intensity of the QDs in the presence and absence of AA, respectively. The regression equation was $y = 1843.5x + 1051.7$, and the corresponding correlation coefficient $R^2 = 0.9962$. The detection limit for AA was estimated to be as low as 0.2 nM. Table S1 lists the comparison of this method and other research for AA testing. Our work provided a lower detection limit, which was superior to those previously reported sensors. This outstanding analytical performance could be attributed to the excellent optical properties of the hydrophilic QDs.



https://doi.org/10.1021/acsomega.4c01045
ACS Omega 2024, 9, 27127−27136

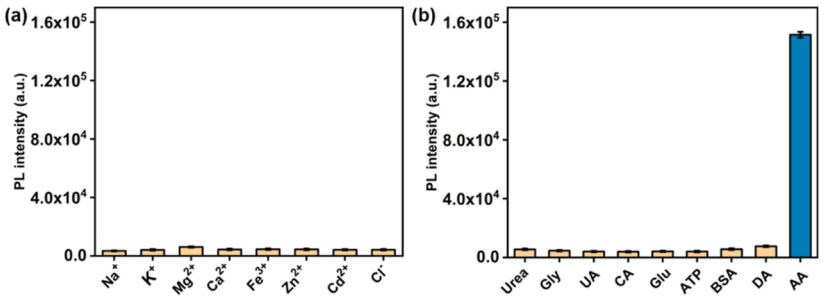


**Figure 6.** Selectivity of the presented sensing system for the determination of AA. Fluorescence change of the QDs after adding 0.3 $\mu$M $Ag^+$ ions in the pre-existence of (a) various ions and (b) biological small molecules. The concentrations of $Na^+$, $K^+$, $Mg^{2+}$, $Ca^{2+}$, $Fe^{3+}$, $Zn^{2+}$, $Cd^{2+}$, $Cl^-$, urea, Gly, UA, CA, Glu, ATP, BSA, and DA were ten times that of AA (200 nM).

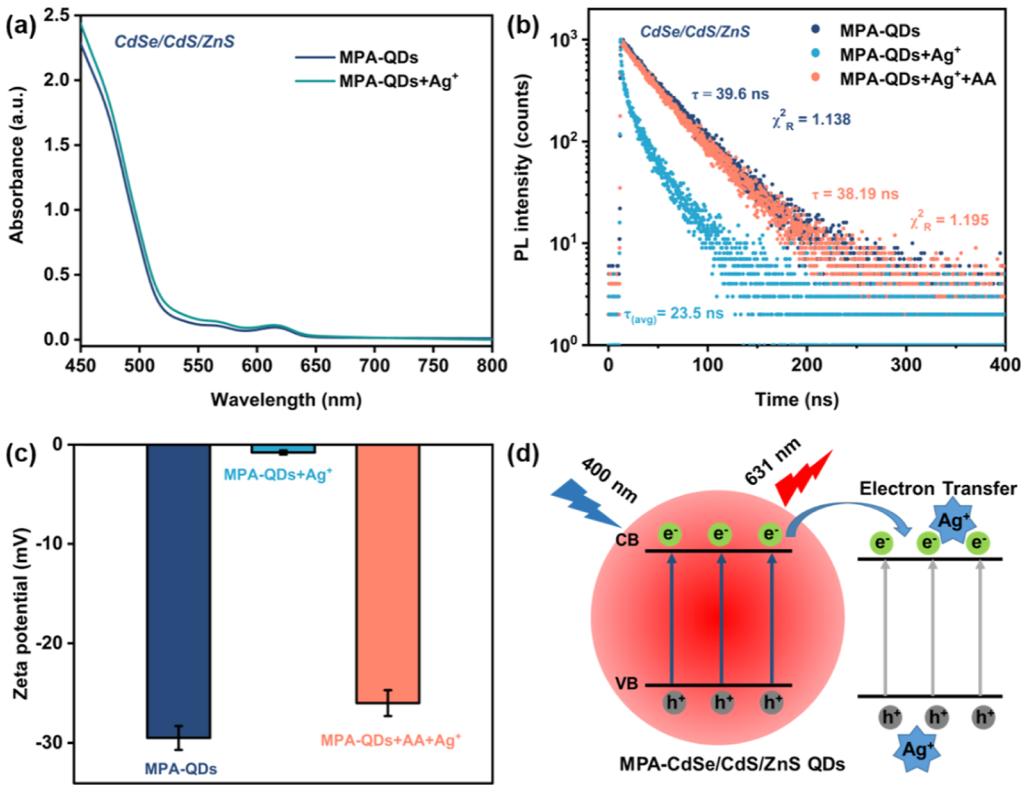


**Figure 7.** (a) UV−visible spectra of the QDs before and after adding $Ag^+$. (b) Time-resolved PL decay curves and (c) zeta potential diagrams of QDs, QDs + $Ag^+$, and QDs + $Ag^+$ + AA. $\tau$ and $\chi_R^2$ represent the fluorescent lifetime and goodness of fit, respectively. (d) Proposed quenching mechanism of the QDs by $Ag^+$ ions.

**3.6. Selectivity of the Developed System.** To further investigate the specificity of the proposed method, the effects of a series of physiologically related reactive species on the intensity of the QDs were evaluated under the same conditions (Figure 6a,b). The fluorescence signal change resulting from ions ($Na^+$, $K^+$, $Mg^{2+}$, $Ca^{2+}$, $Fe^{3+}$, $Zn^{2+}$, $Cd^{2+}$, and $Cl^-$) and biological small molecules (urea, Gly, UA, CA, Glu, ATP, BSA, and DA) were ignorable, even if their concentrations were 10-fold higher than AA. These results demonstrated that this detection system showed excellent selectivity for AA by the fluorescence "on−off−on" process. Accordingly, the QDs/$Ag^+$ hybrid system could be regarded as an ultrasensitive and selective fluorescence sensing platform for AA detection.

**3.7. Fluorescence Quenching Mechanism.** Previous reports had revealed that metal ions were fluorescence quenchers via nonradiative ground-state complex formation,[48] aggregation,[25] inner filter effect,[49] fluorescence resonance energy transfer,[50] and electron transfer.[51] As shown in Figure S9, the fluorescence spectrum of the QDs and the absorption spectrum of $Ag^+$ ions were absence overlapped. Thus, the fluorescence quenching mechanism could not be energy transfer. Moreover, Figure S10 shows that the particle size of the QDs upon the addition of $Ag^+$ did not change, demonstrating that the PL quenching was not due to the aggregation. The peak locations of the absorption and fluorescence spectra of the QDs remained almost invariant in the presence of $Ag^+$ ions (Figures 5a and 7a). Thus, there was no possibility of desorption of the thiolate ligand from the surface of the QDs. To further investigate the quenching mechanism, the fluorescence lifetime experiments were carried out (Figure 7b). The PL lifetime of the QDs was distinctly decreased from 39.6 to 23.5 ns in the presence of $Ag^+$ ions. However, after adding AA, the PL lifetime of the QDs was significantly recovered. These results revealed that the


https://doi.org/10.1021/acsomega.4c01045
ACS Omega 2024, 9, 27127−27136

quenching mechanism of the QDs by $Ag^+$ ions was dynamic quenching. Further, the zeta potential of the QDs before and after adding $Ag^+$ ions was measured (Figure 7c). The zeta potential increased from −29.7 to −0.8 mV when $Ag^+$ ions were added into the QD solution; originating from the QD surface functional groups, they were negatively charged, $Ag^+$ ions were tended to coalesce with the surface carboxyl functional groups. After adding AA, the zeta potential was decreased. Accordingly, the fluorescence quenching mechanism was considered to be electron transfer, which induced the disruption of radiative electron−hole recombination. In order to facilitate the understanding, the detection mechanism is depicted in Figure 7d.

**3.8. Detection of AA in Real Samples.** Orange beverages were selected for exploration to prove that the developed sensing system had practical applicability for AA detection in real samples. These orange beverages were diluted in different amounts with deionized water (pH 11). Based on the results from Figures 5a and S11, the calculated amounts of AA were 0.75 and 0.4 mM, respectively. Thus, the proposed method was suitable for the analysis of AA in real samples.

## 4. CONCLUSIONS

In conclusion, we successfully synthesized the high-quality water-soluble MPA-CdSe/CdS/ZnS QDs with high PL QY and monoexponential PL decay dynamics by rational surface passivation with wide-band gap shells. The fluorescence of the QDs was distinctly quenched once $Ag^+$ ions were added through the electron transfer. A highly sensitive and low-cost fluorescent sensor was successfully developed for AA detection based on the "on−off−on" strategy, originating from the redox reaction between $Ag^+$ ions and AA. The detection limit of AA could be as low as 0.2 nM, which was much lower than that of previously reported methods. This work could provide a guide for designing an excellent optical performance fluorescent probe based on water-soluble QDs.

## ■ ASSOCIATED CONTENT

### Supporting Information

The Supporting Information is available free of charge at https://pubs.acs.org/doi/10.1021/acsomega.4c01045.

TEM images, XRD pattern, UV−vis absorption, fluorescence spectra, PL decay curves, absolute PL quantum yields, fluorescence stability, photographs of the sensor, effect of pH on the sensor, fluorescence quenching mechanism, real sample analysis, and comparison of the detection performance (PDF)

## ■ AUTHOR INFORMATION


### Corresponding Authors

**Yang Li** − *School of Physics and Optoelectronic Engineering, Hangzhou Institute for Advanced Study, University of Chinese Academy of Sciences, Hangzhou, Zhejiang 310024, China; University of Chinese Academy of Sciences, Beijing 100049, China;* orcid.org/0000-0002-8907-5388; Email: ly@ucas.ac.cn

**Xiaoqi Hou** − *School of Chemistry and Material Science, Hangzhou Institute for Advanced Study, University of Chinese Academy of Sciences, Hangzhou, Zhejiang 310024, China; University of Chinese Academy of Sciences, Beijing 100049, China;* orcid.org/0000-0002-5449-2034; Email: houxiaoqi@ucas.ac.cn

### Authors

**Xingchang Lu** − *Hunan Provincial Key Laboratory of Micro & Nano Materials Interface Science, College of Chemistry and Chemical Engineering, Central South University, Changsha, Hunan 410083, China*

**Zheng Wang** − *School of Chemistry and Material Science, Hangzhou Institute for Advanced Study, University of Chinese Academy of Sciences, Hangzhou, Zhejiang 310024, China; University of Chinese Academy of Sciences, Beijing 100049, China*

**Jianxiu Wang** − *Hunan Provincial Key Laboratory of Micro & Nano Materials Interface Science, College of Chemistry and Chemical Engineering, Central South University, Changsha, Hunan 410083, China*

Complete contact information is available at: https://pubs.acs.org/10.1021/acsomega.4c01045


### Author Contributions

X.L. contributed to conceptualization, investigation, formal analysis, and writing the original draft. Z.W. contributed to investigation, validation, and performing the experiments. J.W. contributed to supervision and funding acquisition. Y.L. contributed to methodology and funding acquisition. X.H. contributed to conceptualization, project administration, writing—review and editing, and funding acquisition.

### Notes

The authors declare no competing financial interest.

## ■ ACKNOWLEDGMENTS

This work was supported by the National Natural Science Foundation of China (22105011, 22076221, and 22005267), the National Key Technologies R&D Program of China (2022YFA1207000), the Basic Public Research Program of Zhejiang Province (LY23B010001 and LGF22B010004), and the Funds of Hangzhou Institute for Advanced Study, UCAS (A05006C019001).

## ■ REFERENCES


(1) Chen, Y. J.; Yan, X. P. Chemical redox modulation of the surface chemistry of CdTe quantum dots for probing ascorbic acid in biological fluids. *Small* **2009**, *5*, 2012−2018.

(2) Zhu, X.; Zhao, T.; Nie, Z.; Liu, Y.; Yao, S. Non-redox modulated fluorescence strategy for sensitive and selective ascorbic acid detection with highly photoluminescent nitrogen-doped carbon nanoparticles via solid-state synthesis. *Anal. Chem.* **2015**, *87*, 8524−8530.

(3) Lin, Z.; Zeng, Q.; Yao, W.; Chen, W.; Cai, C.; Yang, J.; Lin, X.; Chen, W. A fluorescence turn-on sensor for ascorbic acid in fruit juice and beverage based on ascorbate oxidase-like activity of citric acid-derived carbon dots. *Food Chem.* **2024**, *437*, 137928.

(4) Zhang, L.; Liu, F.; Sun, X.; Wei, G. F.; Tian, Y.; Liu, Z. P.; Huang, R.; Yu, Y.; Peng, H. Engineering carbon nanotube fiber for real-time quantification of ascorbic acid levels in a live rat model of Alzheimer's disease. *Anal. Chem.* **2017**, *89*, 1831−1837.

(5) Gao, X.; Zhou, X.; Ma, Y.; Qian, T.; Wang, C.; Chu, F. Facile and cost-effective preparation of carbon quantum dots for $Fe^{3+}$ ion and ascorbic acid detection in living cells based on the "on-off-on" fluorescence principle. *Appl. Surf. Sci.* **2019**, *469*, 911−916.

(6) Xu, Y. L.; Niu, X. Y.; Chen, H. L.; Zhao, S. G.; Chen, X. G. Switch-on fluorescence sensor for ascorbic acid detection based on $MoS_2$ quantum dots-$MnO_2$ nanosheets system and its application in fruit samples. *Chin. Chem. Lett.* **2017**, *28*, 338−344.

(7) Zhi, L.; Li, M.; Zhang, S.; Tu, J.; Lu, X. One stone with four birds: methylene blue decorated oxygen-vacancy-rich $MnO_2$ nanosheets for multimode detection of ascorbic acid. *Sens. Actuators, B* **2022**, *354*, 131106.

(8) Abellán-Llobregat, A.; González-Gaitán, C.; Vidal, L.; Canals, A.; Morallón, E. Portable electrochemical sensor based on 4-amino-benzoic acid-functionalized herringbone carbon nanotubes for the determination of ascorbic acid and uric acid in human fluids. *Biosens. Bioelectron.* **2018**, *109*, 123−131.
(9) Zhu, Q.; Bao, J.; Huo, D.; Yang, M.; Hou, C.; Guo, J.; Chen, M.; Fa, H.; Luo, X.; Ma, Y. 3D Graphene hydrogel gold nanoparticles nanocomposite modified glassy carbon electrode for the simultaneous determination of ascorbic acid, dopamine and uric acid. *Sens. Actuators, B* **2017**, *238*, 1316−1323.
(10) Li, Q.; Huo, C.; Yi, K.; Zhou, L.; Su, L.; Hou, X. Preparation of flake hexagonal BN and its application in electrochemical detection of ascorbic acid, dopamine and uric acid. *Sens. Actuators, B* **2018**, *260*, 346−356.
(11) Chen, H.; Li, R.; Lin, L.; Guo, G.; Lin, J. M. Determination of L-ascorbic acid in human serum by chemiluminescence based on hydrogen peroxide-sodium hydrogen carbonate-CdSe/CdS quantum dots system. *Talanta* **2010**, *81*, 1688−1696.
(12) Wang, H.; Pu, G.; Devaramani, S.; Wang, Y.; Yang, Z.; Li, L.; Ma, X.; Lu, X. Bimodal electrochemiluminescence of G-CNQDs in the presence of double coreactants for ascorbic acid detection. *Anal. Chem.* **2018**, *90*, 4871−4877.
(13) Garnero, C.; Longhi, M. Development of HPLC and UV spectrophotometric methods for the determination of ascorbic acid using hydroxypropyl-$\beta$-cyclodextrin and triethanolamine as photo-stabilizing agents. *Anal. Chim. Acta* **2010**, *659*, 159−166.
(14) Li, Y.; Javed, R.; Li, R.; Zhang, Y.; Lang, Z.; Zhao, H.; Liu, X.; Cao, H.; Ye, D. A colorimetric smartphone-based sensor for on-site AA detection in tropical fruits using Fe-P/N C single-atom nanoenzyme. *Food Chem.* **2023**, *406*, 135017.
(15) Wu, A.; Ding, H.; Zhang, W.; Rao, H.; Wang, L.; Chen, Y.; Lu, C.; Wang, X. A colorimetric and fluorescence turn-on probe for the detection of ascorbic acid in living cells and beverages. *Food Chem.* **2021**, *363*, 130325.
(16) Hong, C.; Chen, L.; Huang, J.; Shen, Y.; Yang, H.; Huang, Z.; Cai, R.; Tan, W. Gold nanoparticle-decorated $MoSe_2$ nanosheets as highly effective peroxidase-like nanozymes for total antioxidant capacity assay. *Nano Res.* **2023**, *16*, 7180−7186.
(17) Wei, Z.; Li, H.; Liu, S.; Wang, W.; Chen, H.; Xiao, L.; Ren, C.; Chen, X. Carbon dots as fluorescent/colorimetric probes for real-time detection of hypochlorite and ascorbic acid in cells and body fluid. *Anal. Chem.* **2019**, *91*, 15477−15483.
(18) Ahmed, F.; Xu, W.; Muzammal Hussain, M.; Ullah Khan, W.; Xiong, H. Bioimaging-guided discrimination of normal/cancer cells using $Ag^+$-mediated red fluorescent carbon dots. *Chem. Eng. J.* **2023**, *477*, 147300.
(19) Wang, H.; Na, X.; Liu, S.; Liu, H.; Zhang, L.; Xie, M.; Jiang, Z.; Han, F.; Li, Y.; Cheng, S.; Tan, M. A novel "turn-on" fluorometric and magnetic bi-functional strategy for ascorbic acid sensing and in vivo imaging via carbon dots-MnO2 nanosheet nanoprobe. *Talanta* **2019**, *201*, 388−396.
(20) Guo, L.; Liu, Y.; Kong, R.; Chen, G.; Liu, Z.; Qu, F.; Xia, L.; Tan, W. A metal-organic framework as selectivity regulator for $Fe^{3+}$ and ascorbic acid detection. *Anal. Chem.* **2019**, *91*, 12453−12460.
(21) Ishii, K.; Kubo, K.; Sakurada, T.; Komori, K.; Sakai, Y. Phthalocyanine-based fluorescence probes for detecting ascorbic acid: phthalocyaninatosilicon covalently linked to TEMPO radicals. *Chem. Commun.* **2011**, *47*, 4932−4934.
(22) Liu, Z. C.; Qi, J. W.; Hu, C.; Zhang, L.; Song, W.; Liang, R. P.; Qiu, J. D. Cu nanoclusters-based ratiometric fluorescence probe for ratiometric and visualization detection of copper ions. *Anal. Chim. Acta* **2015**, *895*, 95−103.
(23) Wang, X.; Wu, P.; Hou, X.; Lv, Y. An ascorbic acid sensor based on protein-modified Au nanoclusters. *Analyst* **2013**, *138*, 229−233.
(24) Mo, Q.; Liu, F.; Gao, J.; Zhao, M.; Shao, N. Fluorescent sensing of ascorbic acid based on iodine induced oxidative etching and aggregation of lysozyme-templated silver nanoclusters. *Anal. Chim. Acta* **2018**, *1003*, 49−55.
(25) Na, W.; Qu, Z.; Chen, X.; Su, X. A turn-on fluorescent probe for sensitive detection of sulfide anions and ascorbic acid by using sulfanilic acid and glutathione functionalized graphene quantum dots. *Sens. Actuators, B* **2018**, *256*, 48−54.
(26) Liu, R.; Yang, R.; Qu, C.; Mao, H.; Hu, Y.; Li, J.; Qu, L. Synthesis of glycine-functionalized graphene quantum dots as highly sensitive and selective fluorescent sensor of ascorbic acid in human serum. *Sens. Actuators, B* **2017**, *241*, 644−651.
(27) Liu, H.; Na, W.; Liu, Z.; Chen, X.; Su, X. A novel turn-on fluorescent strategy for sensing ascorbic acid using graphene quantum dots as fluorescent probe. *Biosens. Bioelectron.* **2017**, *92*, 229−233.
(28) Shi, H.; Chen, L.; Niu, N. An off-on fluorescent probe based on graphene quantum dots intercalated hydrotalcite for determination of ascorbic acid and phytase. *Sens. Actuators, B* **2021**, *345*, 130353.
(29) Luo, X.; Zhang, W.; Han, Y.; Chen, X.; Zhu, L.; Tang, W.; Wang, J.; Yue, T.; Li, Z. N,S co-doped carbon dots based fluorescent "on-off-on" sensor for determination of ascorbic acid in common fruits. *Food Chem.* **2018**, *258*, 214−221.
(30) Li, L.; Wang, C.; Liu, K.; Wang, Y.; Liu, K.; Lin, Y. Hexagonal cobalt oxyhydroxide-carbon dots hybridized surface: high sensitive fluorescence turn-on probe for monitoring of ascorbic acid in rat brain following brain ischemia. *Anal. Chem.* **2015**, *87*, 3404−3411.
(31) Lv, X.; Man, H.; Dong, L.; Huang, J.; Wang, X. Preparation of highly crystalline nitrogen-doped carbon dots and their application in sequential fluorescent detection of $Fe^{3+}$ and ascorbic acid. *Food Chem.* **2020**, *326*, 126935.
(32) Zhu, Y.; Deng, X.; Chen, J.; Hu, Z.; Wu, F. Coffee grounds-derived carbon quantum dots as peroxidase mimetics for colorimetric and fluorometric detection of ascorbic acid. *Food Chem.* **2023**, *429*, 136957.
(33) Wang, M.; Shi, R.; Gao, M.; Zhang, K.; Deng, L.; Fu, Q.; Wang, L.; Gao, D. Sensitivity fluorescent switching sensor for Cr (VI) and ascorbic acid detection based on orange peels-derived carbon dots modified with EDTA. *Food Chem.* **2020**, *318*, 126506.
(34) Zhang, K.; Guo, J.; Nie, J.; Du, B.; Xu, D. Ultrasensitive and selective detection of $Cu^{2+}$ in aqueous solution with fluorescence enhanced CdSe quantum dots. *Sens. Actuators, B* **2014**, *190*, 279−287.
(35) Ahn, N.; Livache, C.; Pinchetti, V.; Klimov, V. I. Colloidal semiconductor nanocrystal lasers and laser diodes. *Chem. Rev.* **2023**, *123*, 8251−8296.
(36) Ma, Z.; Sun, Z.; Yang, H.; Wang, Z.; Ren, F.; Yin, N.; Chen, Q.; Zhang, Y.; Li, C.; Chen, L.; Wang, Q. Interface-mediation-enabled high-performance near-infrared AgAuSe quantum dot light-emitting diodes. *J. Am. Chem. Soc.* **2023**, *145*, 24972−24980.
(37) Jang, E.; Jang, H. Review: quantum dot light-emitting diodes. *Chem. Rev.* **2023**, *123*, 4663−4692.
(38) Gill, R.; Zayats, M.; Willner, I. Semiconductor quantum dots for bioanalysis. *Angew. Chem., Int. Ed.* **2008**, *47*, 7602−7625.
(39) Hou, X.; Kang, J.; Qin, H.; Chen, X.; Ma, J.; Zhou, J.; Chen, L.; Wang, L.; Wang, L.; Peng, X. Engineering Auger recombination in colloidal quantum dots via dielectric screening. *Nat. Commun.* **2019**, *10*, 1750.
(40) Hu, Z.; Liu, S.; Qin, H.; Zhou, J.; Peng, X. Oxygen stabilizes photoluminescence of CdSe/CdS core/shell quantum dots via deionization. *J. Am. Chem. Soc.* **2020**, *142*, 4254−4264.
(41) Gupta, R.; Peveler, W. J.; Lix, K.; Algar, W. R. Comparison of semiconducting polymer dots and semiconductor quantum dots for smartphone-based fluorescence assays. *Anal. Chem.* **2019**, *91*, 10955−10960.
(42) Jun, B.-H.; Hwang, D. W.; Jung, H. S.; Jang, J.; Kim, H.; Kang, H.; Kang, T.; Kyeong, S.; Lee, H.; Jeong, D. H.; et al. Ultrasensitive, biocompatible, quantum-dot-embedded silica nanoparticles for bioimaging. *Adv. Funct. Mater.* **2012**, *22*, 1843−1849.
(43) Huang, L.; Zhang, Y.; Liao, T.; Xu, K.; Jiang, C.; Zhuo, D.; Wang, Y.; Wen, H. M.; Wang, J.; Ao, L.; Hu, J. Compact Magneto-Fluorescent Colloids by Hierarchical Assembly of Dual-Components in Radial Channels for Sensitive Point-of-Care Immunoassay. *Small* **2021**, *17*, 2100862.


https://doi.org/10.1021/acsomega.4c01045
*ACS Omega* 2024, 9, 27127−27136

(44) Yang, H. Y.; Fu, Y.; Jang, M. S.; Li, Y.; Lee, J. H.; Chae, H.; Lee, D. S. Multifunctional polymer ligand interface CdZnSeS/ZnS quantum dot/Cy3-labeled protein pairs as sensitive FRET sensors. *ACS Appl. Mater. Interfaces* **2016**, *8*, 35021−35032.
(45) Li, J.; Lv, Y.; Li, N.; Wu, R.; Xing, M.; Shen, H.; Li, L. S.; Chen, X. Robust synthesis of bright multiple quantum dot-embedded nanobeads and its application to quantitative immunoassay. *Chem. Eng. J.* **2019**, *361*, 499−507.
(46) Cao, Z.; Shu, Y.; Qin, H.; Su, B.; Peng, X. Quantum dots with highly efficient, stable, and multicolor electrochemiluminescence. *ACS Cent. Sci.* **2020**, *6*, 1129−1137.
(47) Hou, X.; Qin, H.; Peng, X. Enhancing dielectric screening for auger suppression in CdSe/CdS quantum dots by epitaxial growth of ZnS shell. *Nano Lett.* **2021**, *21*, 3871−3878.
(48) Zhong, Y.; Zou, Y.; Yang, X.; Lu, Z.; Wang, D. Ascorbic acid detector based on fluorescent molybdenum disulfide quantum dots. *Microchim. Acta* **2022**, *189*, 19.
(49) Li, P.; Liang, N.; Liu, C.; Xia, L.; Qu, F.; Song, Z. L.; Kong, R. M. Silver ion-regulated ratiometric fluorescence assay for alkaline phosphatase detection based on carbon dots and o-phenylenediamine. *Spectrochim. Acta, Part A* **2022**, *282*, 121682.
(50) Li, L.; Wang, C.; Luo, J.; Guo, Q.; Liu, K.; Liu, K.; Zhao, W.; Lin, Y. $Fe^{3+}$-functionalized carbon quantum dots: a facile preparation strategy and detection for ascorbic acid in rat brain microdialysates. *Talanta* **2015**, *144*, 1301−1307.
(51) Yan, X.; Ma, J.; Yu, K.; Li, J.; Yang, L.; Liu, J.; Wang, J.; Cai, L. Highly green fluorescent $Nb_2C$ MXene quantum dots for $Cu^{2+}$ ion sensing and cell imaging. *Chin. Chem. Lett.* **2020**, *31*, 3173−3177.



https://doi.org/10.1021/acsomega.4c01045
*ACS Omega* 2024, 9, 27127−27136